Molecular Cell, Volume *69*

Supplemental Information

Structural Basis for NusA

Stabilized Transcriptional Pausing

Xieyang Guo, Alexander G. Myasnikov, James Chen, Corinne Crucifix, Gabor Papai, Maria Takacs, Patrick Schultz, and Albert Weixlbaumer

Table S1: Superposition of paused RNAP complexes to measure shelf/clamp rotation, related to Figure 7

Models were aligned using PyMOL's align function based on protein backbone of core module (Table S2)

	Number of atoms used (core module)	RMSD (Å)
ePEC[1] to EC core[2]	4554	1.05
***his*PEC[1] to EC core[2]**	4442	0.83
PEC-NusA[3] to EC core[2]	4490	1.16
***his*PEC-NusA[3] to EC core[2]**	4531	1.12

[1]Kang et al., submitted
[2]Kang et al., 2017
[3]present work

Superposition of pre-aligned models (based on core) to derive shelf/clamp rotation using PyMOL's align function and output of transformation matrix (see also Table S2)

	Number of atoms used (shelf/clamp)	RMSD (Å)	Shelf/Clamp rotation (°)
EC[1] to ePEC[2]	3537	1.011	~0.5
EC[1] to *his*PEC[2]	4079	1.024	~3.6
EC[1] to PEC-NusA[3]	4421	1.359	~2.6
EC[1] to *his*PEC-NusA[3]	4406	1.238	~4.8

[1]Kang et al., 2017
[2]Kang et al., submitted
[3]present work

Table S2: Definitions of structural modules of *E. coli* RNAP used in the present work, related to Figure 7

Module	Subunits	*E. coli* residues (chain ID, residue number)
Core	2α β β'	A1- A234, B1-B234 C10-C26, C514-C828, C1071-C1235 D504-D771
Shelf	β β' ω	C1244-C1309 D346-D499 D805-D1317 D1358-D1407 all
β1	β	C31-C139 C456-C512
β2	β	C143-C448
β-flap	β	C829-937, C1040-1059
β-flap-tip	β	C891-C912
β-flap-tip-helix	β	C897-C907
Clamp	β β'	C1296-C1342 D1-D329 D1321-D1344
Lid	β'	D251-D263
β'-coiled-coil (clamp helices)	β'	D264-D332
Bridge helix	β'	D770-D804
Switch2	β'	D330-D345
β'-dock	β'	D369-D420
β'-zinc finger	β'	D66-D95
Sequence insertion 1 (SI1)	β	C226-C339
Sequence insertion 3 (SI3)	β'	D946-D1126

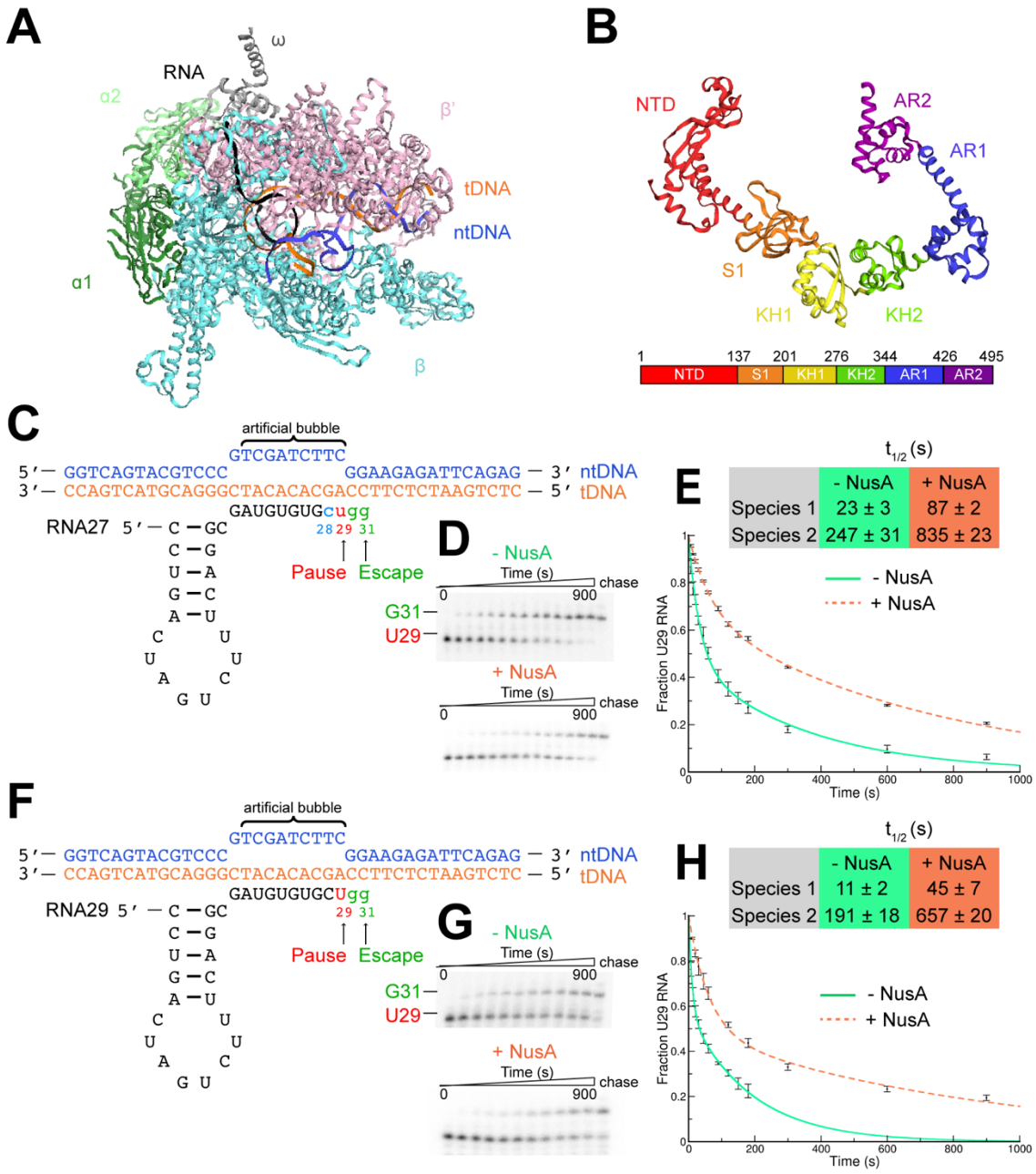

Figure S1. Overview of RNAP, NusA and *his*PEC pause kinetics, related to Figure 1

(A) An overview of the *E.coli* RNAP EC structure is shown as a backbone ribbon, with color-coded subunits and nucleic acids.

(B) An overview of the *E. coli* NusA structure is shown as an α-carbon backbone ribbon, with color-coded domains.

(C) Schematic of the nucleic acid scaffold (ntDNA blue, tDNA orange, RNA black) used to assemble an EC upstream of the pause site to measure pause escape kinetics. Using ^{32}P-α-CTP

and UTP, internally labeled *his*PECs were formed by extending RNA27 stepwise to C28 (blue) and to the target pause site U29 (red). Pause escape rates for *his*PECs were determined by adding GTP and measuring the RNA extension to position G31 (green).

(D) The *his*PEC responds to NusA: *his*PECs (1 μM, formed as described in C) were elongated with GTP (100 μM) in the absence (green) or presence (orange) of NusA (4 μM). Aliquots were removed at different time points and RNA products were separated on a 15% denaturing polyacrylamide gel. The gel was quantified as described in the Methods section. A representative gel is shown here.

(E) The fraction of RNA29 remaining from at least three independent experiments was plotted as a function of time. The rate of pause escape was determined by nonlinear regression of [U29] versus time using a double exponential decay. Double exponential decay suggested two species of RNAP with different pause half-lives ($t_{1/2}$) as seen in the table. In both species NusA enhanced pause duration 3-4 fold. Data are represented as mean ± SEM.

(F) Schematic of the nucleic acid scaffold (ntDNA blue, tDNA orange, and RNA29 black) used to assemble the *his*PEC directly at the pause site for cryo-EM studies. The target pause site (U29, red), and RNA products after pause escape (position G30 and G31, green) are highlighted.

(G) Directly assembled *his*PECs respond to NusA in cryoEM sample buffer conditions: *his*PECs (1 μM) containing end-labeled RNA29 (^{32}P-γ-ATP) were elongated with GTP (100 μM) in the absence (green) or presence (orange) of NusA (4 μM). Aliquots were removed, and RNA products were separated on a 15% denaturing polyacrylamide gel. The gel was quantified as described in the Methods section. A representative gel is shown here.

(H) The fraction of RNA29 remaining from at least three independent experiments was plotted as a function of time. The rate of pause escape was determined by nonlinear regression of [U29] versus time using a double exponential decay. Double exponential decay suggested two species of RNAP with different pause half-lives ($t_{1/2}$) as seen in the table. In both species NusA has enhanced pause duration 3-4 fold. Data are represented as mean ± SEM.

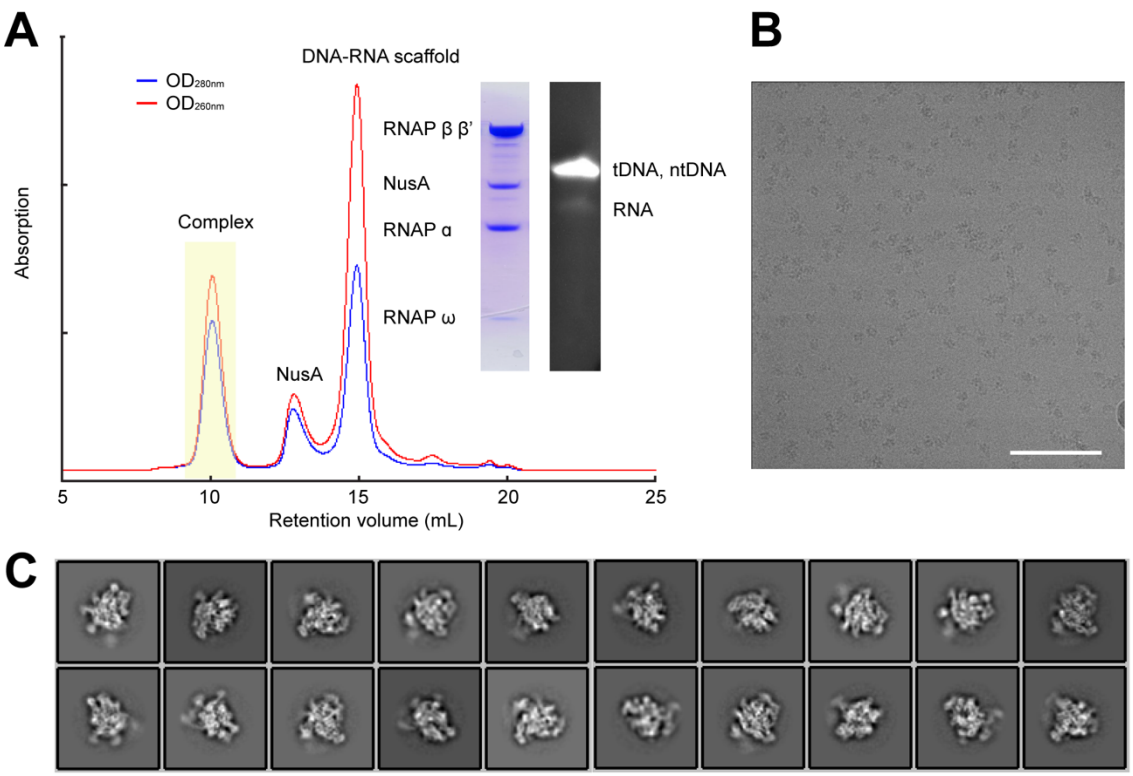

Figure S2. Complex purification and cryo-EM analysis, related to Figure 1

(A) Paused *E. coli* RNAP elongation complexes were assembled *in vitro* directly at the *his*-pause site using an excess of NusA and nucleic acid ligands. Complexes were stable and could be purified by size exclusion chromatography. A Coomassie-stained SDS-PAGE and a urea denaturing gel (15% polyacrylamide) stained by ethidium bromide of the pooled complex peak fractions reveals all subunits of RNAP, NusA and nucleic acid ligands.

(B) Optimized buffer conditions lead to an even distribution of particles, as seen in this exemplary micrograph. The scale bar is 100 nm.

(C) Representative 2D class averages of the particles.

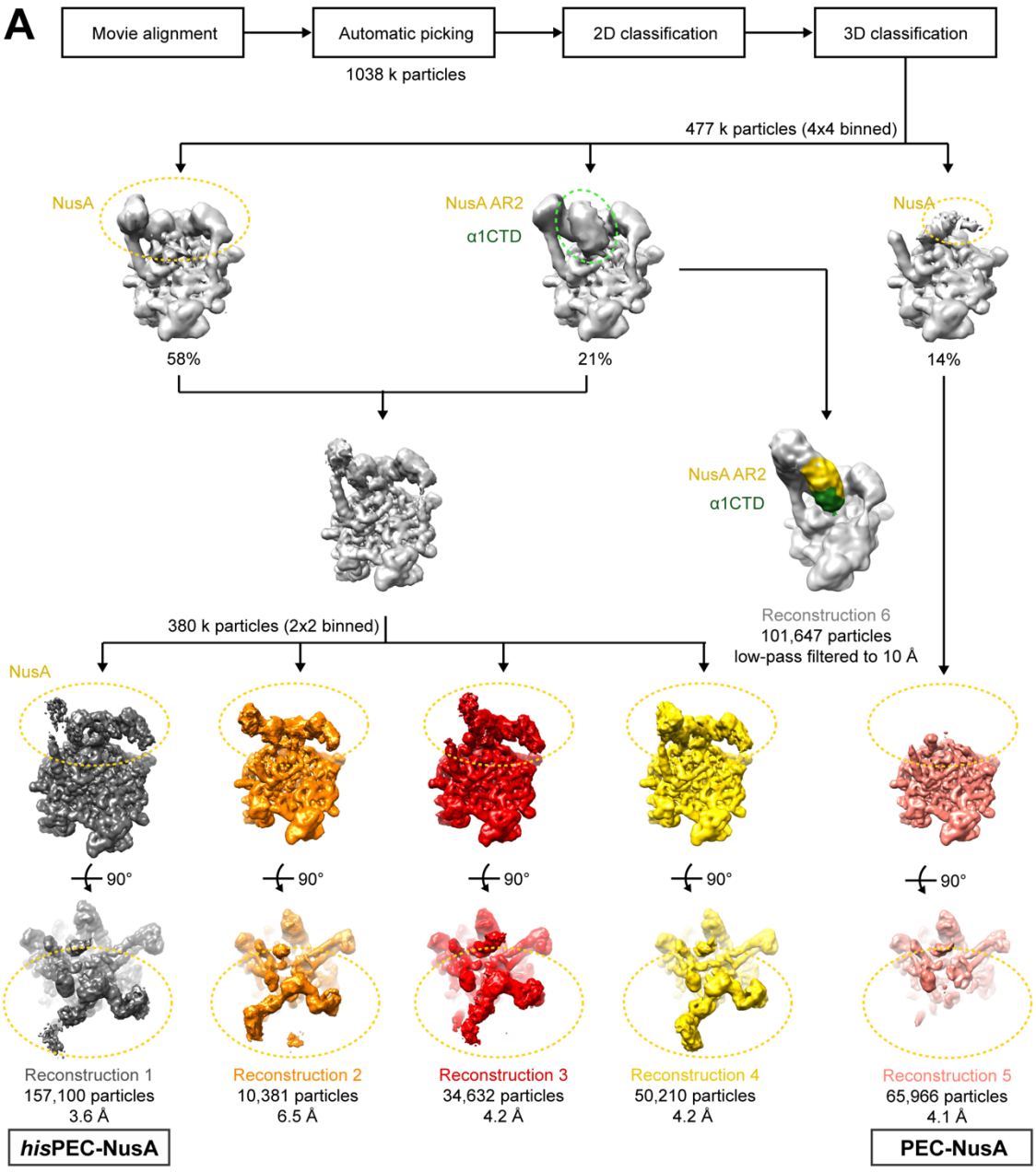
A
Movie alignment
Automatic picking
1038 k particles
2D classification
3D classification
477 k particles (4x4 binned)
NusA
NusA AR2
α1CTD
NusA
58%
21%
14%
NusA AR2
α1CTD
Reconstruction 6
101,647 particles
low-pass filtered to 10 Å
380 k particles (2x2 binned)
NusA
90°
90°
90°
90°
90°
Reconstruction 1
157,100 particles
3.6 Å
hisPEC-NusA
Reconstruction 2
10,381 particles
6.5 Å
Reconstruction 3
34,632 particles
4.2 Å
Reconstruction 4
50,210 particles
4.2 Å
Reconstruction 5
65,966 particles
4.1 Å
PEC-NusA

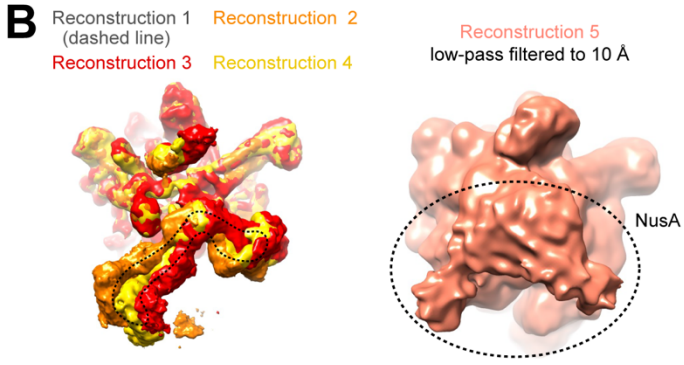
B
Reconstruction 1
(dashed line)
Reconstruction 2
Reconstruction 3
Reconstruction 4
Reconstruction 5
low-pass filtered to 10 Å
NusA

Figure S3. Classification and refinement flow diagram, related to Figure 2.

(A) Processing and classification tree with the resulting 6 reconstructions: Reconstruction 1 shows highest resolution for RNAP core and represents NusA average; Reconstruction 2, 3, and 4 show extremes of NusA movement relative to RNAP; Reconstruction 5 shows very weak density for NusA; Reconstruction 6 low-pass filtered to 10 Å shows density for RNAP α2 CTD and NusA AR2. Resolution of the resulting refined map is indicated below each class.

(B) Superposition of four reconstructions. Reconstruction 1 (black dashed line) is the average of different NusA orientations relative to RNAP (reconstructions 2, 3, and 4; left). Reconstruction 5 low-pass filtered to 10 Å shows density for NusA (right).

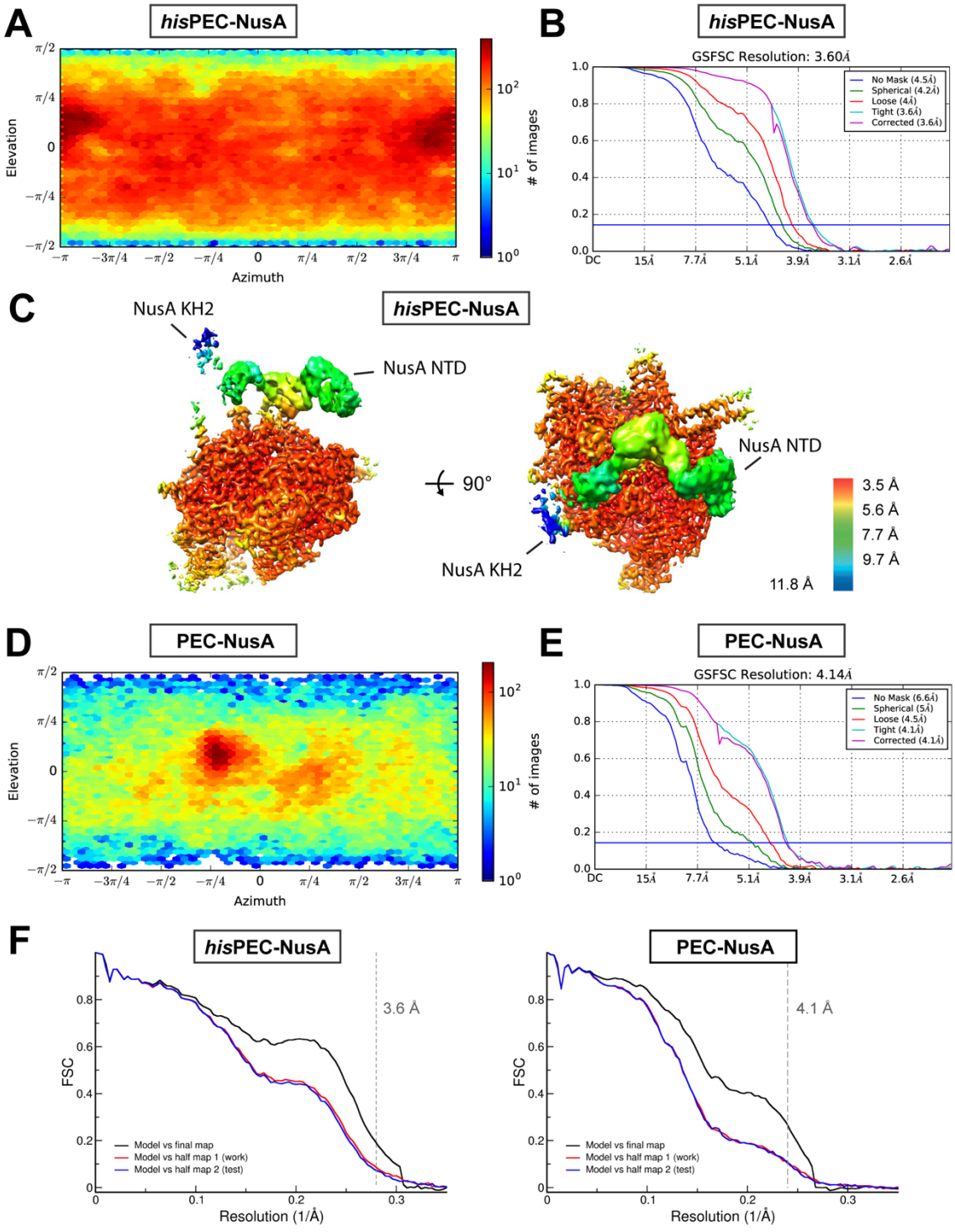
A
hisPEC-NusA
Elevation
Azimuth
# of images
B
hisPEC-NusA
GSFSC Resolution: 3.60Å
No Mask (4.5Å)
Spherical (4.2Å)
Loose (4Å)
Tight (3.6Å)
Corrected (3.6Å)
C
hisPEC-NusA
NusA KH2
NusA NTD
90°
NusA NTD
NusA KH2
3.5 Å
5.6 Å
7.7 Å
9.7 Å
11.8 Å
D
PEC-NusA
Elevation
Azimuth
# of images
E
PEC-NusA
GSFSC Resolution: 4.14Å
No Mask (6.6Å)
Spherical (5Å)
Loose (4.5Å)
Tight (4.1Å)
Corrected (4.1Å)
F
hisPEC-NusA
3.6 Å
FSC
Model vs final map
Model vs half map 1 (work)
Model vs half map 2 (test)
Resolution (1/Å)
PEC-NusA
4.1 Å
FSC
Model vs final map
Model vs half map 1 (work)
Model vs half map 2 (test)
Resolution (1/Å)

Figure S4. Cryo-EM reconstruction of *his*PEC-NusA and PEC-NusA, related to Figure 1 and Figure 7

(A) Angular distribution plot shows random particle orientation of the *his*PEC-NusA reconstruction.

(B) Fourier shell correlation (FSC) plot for half-maps of the *his*PEC-NusA reconstruction with 0.143 FSC criteria indicated. The final resolution is determined to be 3.6 Å.

(C) Local resolution of the *his*PEC-NusA reconstruction. In the core of the complex we reach 3.5Å but at the periphery and in particular in the region of NusA, local resolution is lower.

(D) Angular distribution plot shows random particle orientation of the PEC-NusA reconstruction.

(E) Fourier shell correlation (FSC) plot for half-maps of the PEC-NusA reconstruction with 0.143 FSC criteria indicated. The final resolution is determined to be 4.1 Å.

(F) Model vs map FSC curves for final model for *his*PEC-NusA and PEC-NusA versus the final map it was refined against (black); of the model refined in the first of the two-independent half maps versus the same map (red; FSC_{work}); and of the model refined in the first of the two-independent half maps versus the second independent half-map (blue; FSC_{test}). The resolution cutoff applied during refinement is shown as a vertical dashed line. The closely matching profiles of FSC_{work} and FSC_{test} indicates that no significant overfitting took place.

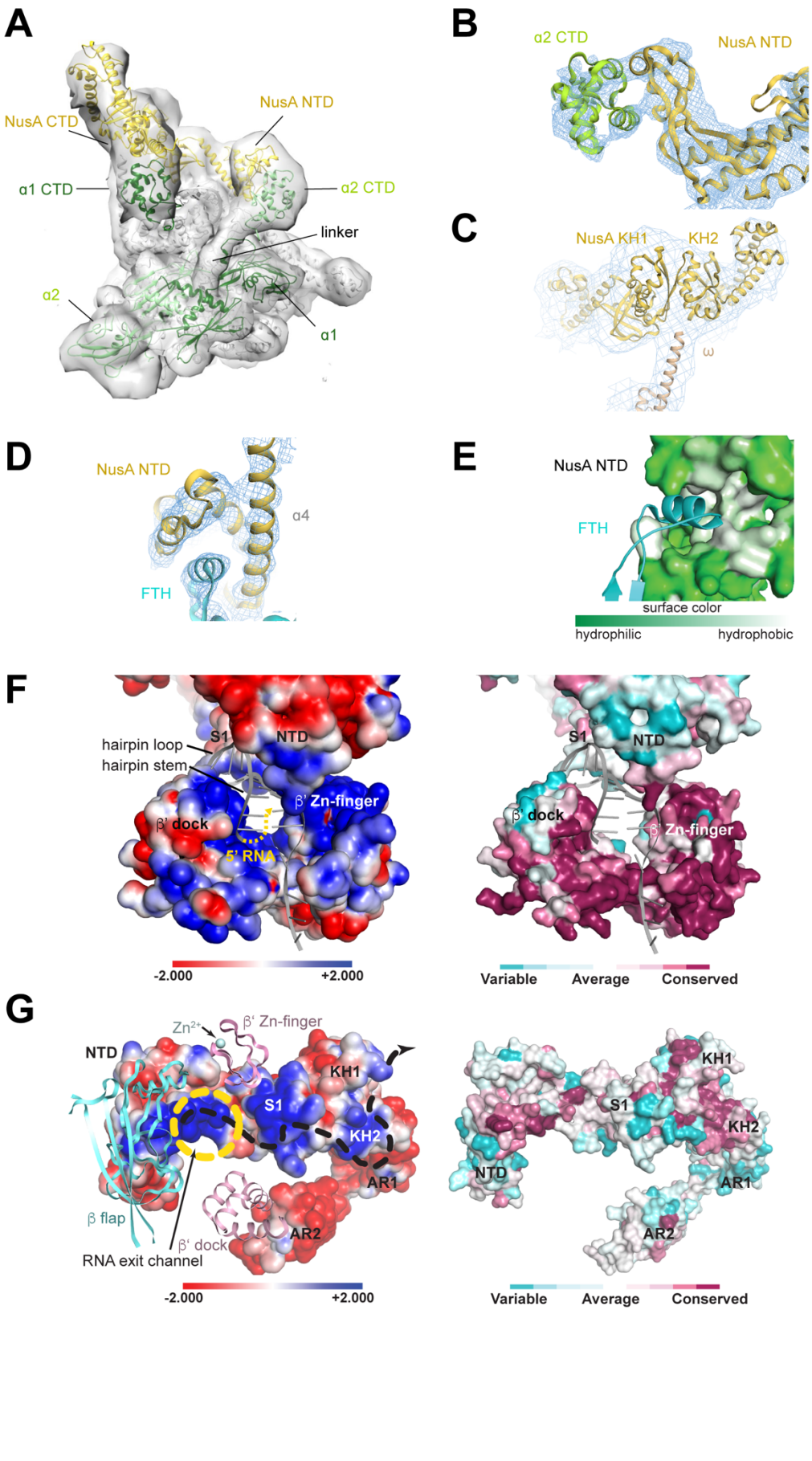
A
NusA CTD
NusA NTD
α1 CTD
α2 CTD
linker
α2
α1
B
α2 CTD
NusA NTD
C
NusA KH1
KH2
ω
D
NusA NTD
α4
FTH
E
NusA NTD
FTH
surface color
hydrophilic
hydrophobic
F
hairpin loop
hairpin stem
S1
NTD
β' Zn-finger
β' dock
5' RNA
-2.000
+2.000
S1
NTD
β' dock
β' Zn-finger
Variable
Average
Conserved
G
Zn2+
β' Zn-finger
NTD
KH1
S1
KH2
AR1
β flap
AR2
β' dock
RNA exit channel
-2.000
+2.000
KH1
S1
KH2
NTD
AR1
AR2
Variable
Average
Conserved

Figure S5. Interactions between NusA and *his*PEC, related to Figure 3

(A) Low-pass filtered map of the *his*PEC-NusA reconstruction 6 (see Figure S3A) (grey envelope) with cartoon representation of NusA (yellow), RNAP α1 subunit (forest) and α2 subunit (lime).

(B) Cryo-EM density (blue mesh) for interaction of NusA-NTD (yellow) with α2-CTD (lime) is shown with cartoon model superimposed.

(C) Cryo-EM density (blue mesh) for the interaction of the RNAP ω–subunit with the interface of the NusA KH1 and KH2 domains with a cartoon model superimposed is shown.

(D) Cryo-EM density (blue mesh) for interaction of NusA-NTD (yellow) with the FTH (cyan) is shown with cartoon model superimposed.

(E) Hydrophobic surface representation of NusA interaction area with RNAP FTH (cyan). The FTH inserts into a hydrophobic pocket.

(F) Electrostatic surface potential of NusA-NTD and S1, RNAP β' dock and β'-zinc finger forming a positively charged pore providing a path for the nascent transcript. Yellow dashed line indicates potential path for 5'-end of the RNA upstream of the hairpin (left). Surface of the pore colored by conservation based on alignment of 30 bacterial phyla (right).

(G) Electrosative surface potential of NusA. Yellow dashed line indicates the RNA exit channel surrounded by β flap, β' dock and β'-zinc finger. Black dashed line represents potential path for RNA along the positive charged surface of NusA (left). Surface of NusA colored by conservation base on alignment of 30 bacterial phyla (right)

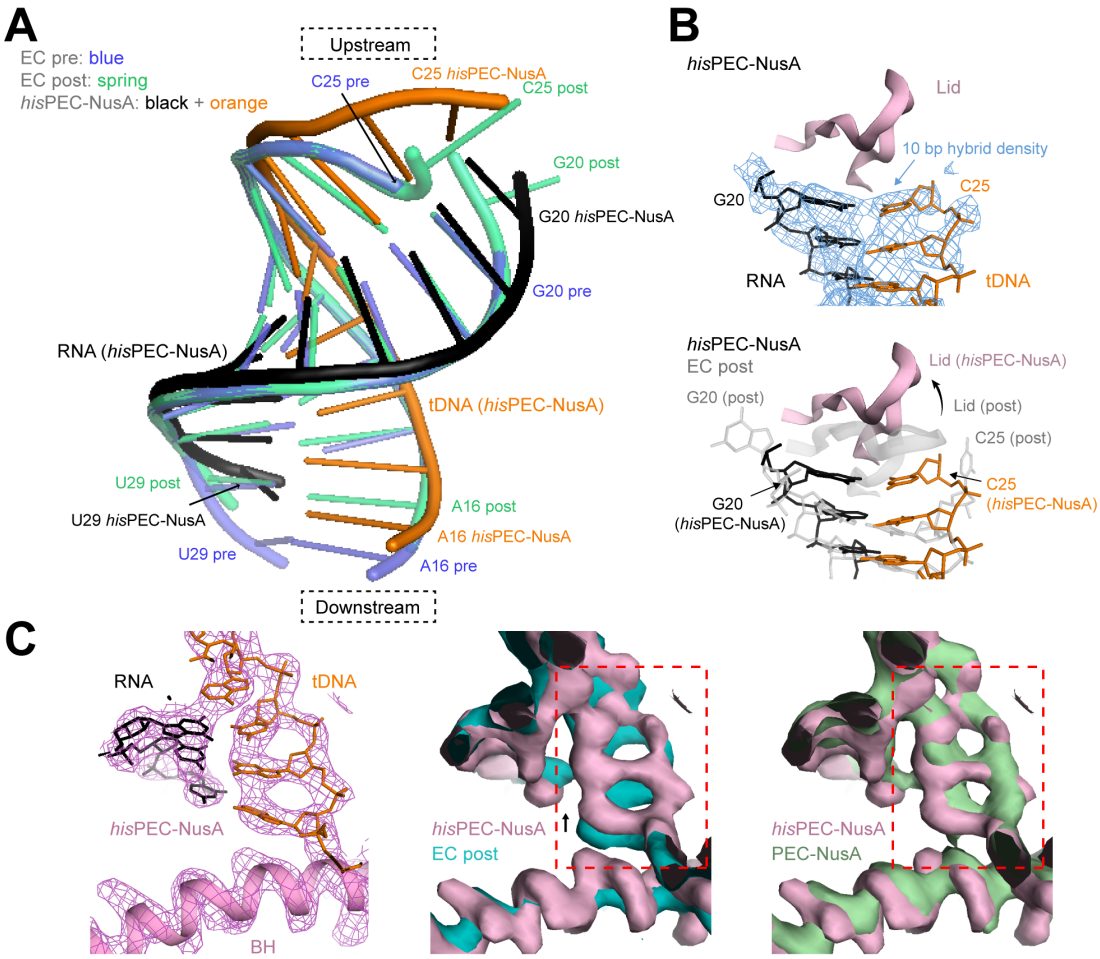

Figure S6. Comparison of the RNA-DNA hybrid in the *his*PEC-NusA with EC structures, related to Figure 6

(A) Comparison of RNA-DNA hybrid between pre-translocated EC (blue), post-translocated EC (spring) and *his*PEC-NusA (tDNA, orange; RNA, black). The two EC hybrids are modeled using the *his*PEC sequence and based on PDB ID 6ALH (Kang et al., 2017).

(B) Representative areas of cryo-EM density (blue mesh) for upstream end of RNA-DNA hybrid showing the -10 base pair with a stick model superimposed (top). Comparison of lid loop (pink) between EC (grey transparent) and *his*PEC-NusA (pink). A superprosition of a modeled pre-translocated hybrid (grey transparent) and the hybrid of the *his*PEC is also shown (color). In the *his*PEC the lid loop moved upstream providing space for the -10 base pair.

(C) Cryo-EM density (pink mesh) of *his*PEC-NusA active site with tDNA (orange), RNA (black) and bridge helix (pink) shown in cartoon (left). Comparison of cryo-EM density of active site between *his*PEC-NusA (pink surface) and post-translocated EC (cyan surface) (PDB ID 6ALH) (Kang et al., 2017) with dashed area showing movement of tDNA (center). Comparison of cryo-EM density of active site between *his*PEC-NusA reconstruction 1 (pink surface) and PEC-NusA reconstruction 5 (lacking hairpin and with weak NusA density, see Figure S3A) (green surface) with dashed area showing no difference between these two reconstruction.

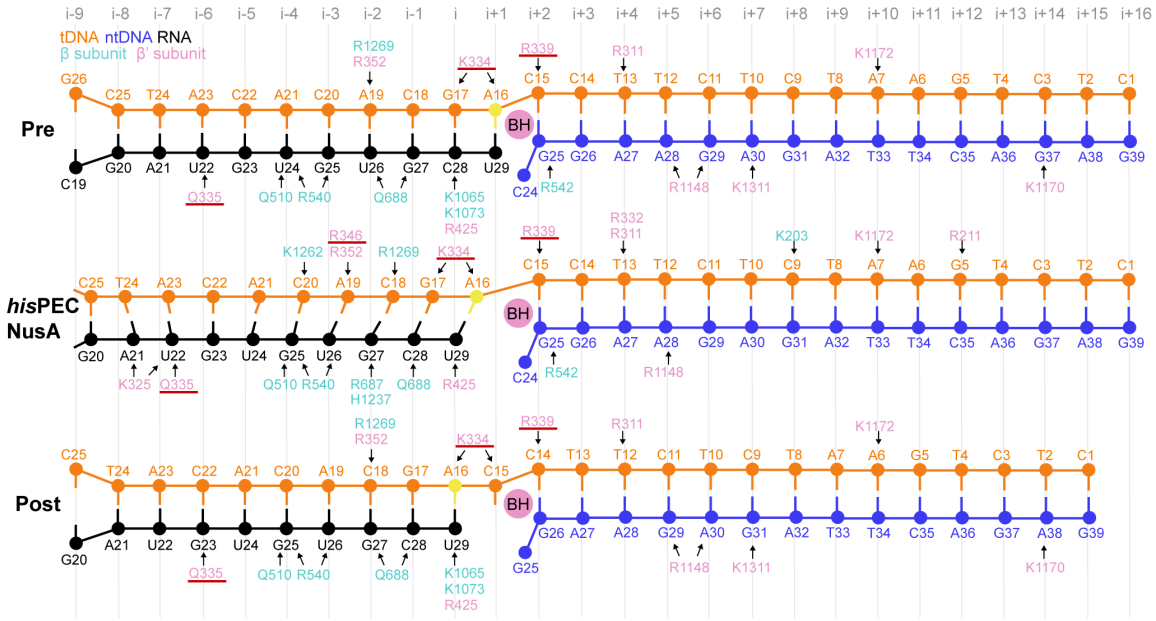

Figure S7. Schematic of RNAP-nucleic acid contacts, related to Figure 6

Schematic illustration of polar interactions between RNAP and the RNA-DNA hybrid and downstream DNA duplex in pre- (top), and post-translocated states (bottom), and for the *his*PEC-NusA (middle). Hybrid movement of the *his*PEC-NusA was estimated using the ribose moieties of the pre- and post-translocation complex as references. Ribose sugars are shown as circles, bases and phosphates are shown as lines. Arrows indicate polar interactions. Grey squares indicate weak interactions (judged by distance). Residues of the RNAP Switch 2 are underlined.